IEEE Access
Multidisciplinary | Rapid Review | Open Access Journal

Received April 19, 2019, accepted May 6, 2019, date of publication May 13, 2019, date of current version May 31, 2019.

Digital Object Identifier 10.1109/ACCESS.2019.2916379

Stiffness Adjustment for a Single-Link Robot Arm Driven by Series Elastic Actuator in Muscle Training

SIQI LI[1], JIAN LI[2], GUIHUA TIAN[3], AND HONGCAI SHANG[3]

[1]Key Laboratory for Bionic Robot and System, School of Mechatronical Engineering, Beijing Institute of Technology, Beijing 100081, China
[2]Key Laboratory for Intelligent Control and Decision on Complex Systems, School of Automation, Beijing Institute of Technology, Beijing 100029, China
[3]Laboratory of Chinese Internal Medicine of Ministry of Education and Beijing, Dongzhimen Hospital, Beijing University of Chinese Medicine, Beijing 100029, China

Corresponding authors: Jian Li (yellowlightlee@163.com) and Guihua Tian (rosetgh@163.com)

This work was supported in part by the Intelligent Equipment and Technology of Automation Research and Development Platform under Grant 2016F2FC007, and in part by the National Key Research and Development Program of China under Grant 2018YFC1707604.

ABSTRACT Series elastic actuators (SEAs) can improve the performance of robots and ensure their safety; therefore, they are widely applied in rehabilitation robots. To effectively exercise muscles in late rehabilitation training, robots utilize different impedance characteristics according to human muscle conditions. In this study, a novel real-time parallel variable-stiffness control method is proposed. The method predicts the muscle stiffness of the human body during the interaction process, and then adjusts the port stiffness of the SEA as needed to improve strength training. The impedance controller is used to meet the port stiffness and stability requirements during interactions. The predictive stiffness control method not only assesses the stiffness of human muscles in real time but also meets the constraint conditions associated with interaction stability, speed, and position. This control structure enables effective and safe strength training. Finally, the experimental results indicate that the stiffness control method based on muscle stiffness prediction can accurately match the port stiffness and provide interaction stability for effective muscle exercise.

INDEX TERMS Series elastic actuator, stiffness predictive algorithm, rehabilitation interactive design.

I. INTRODUCTION

Muscle training is the essence of physical exercise. Series elastic actuator (SEA) is a flexible device with cascading elastic parts involved with the motor and load [1]. SEAs can absorb shocks, reduce output impedance and provide high-precision torque output [2]–[5]. Therefore, they are widely applied in robots, such as Baxter robots [6], Exoskeleton LOPES [7] and other rehabilitation/booster robots [8], to improve security and the ease of human-machine interactions.

Stiffness adjustment is usually accomplished via two types: mechanical on hardware and control on software. With reference to DLR-HASy [9], all actuators of the arm are variable stiffness actuators (VSAs) [10], [11]. The primary advantage of VSAs is their improved task adaptability due to their adjustable stiffness [12]–[15]. However, it is necessary for the VSA design to incorporate an independent spring stiffness mechanism that is adjustable, which will significantly increase its complexity, cost and size [16], [17]. Contrary to the adjustable compliance VSA-joint, the fixed compliance SEA-joint is capable of changing its stiffness using software.

The primary purpose of stiffness adjustment is to accomplish various interactive tasks. To achieve adequate interaction behavior, Hogan proposed the concept of an impedance control method and an interaction port [18]. An interaction port can exchange energy with the environment [19], while interactive control involves specifying a dynamic relationship between motion and force at the port [20], [21]. A variety of interaction control schemes have been developed for robotic manipulators with SEA joints, including adaptive control [22], [23], backstepping control [24], [25], optimal control [26], multi-modal control [27], and model predictive control [28]–[30].

Cascade structures have been widely applied in SEA control [5], [31]–[34], among which torque embedded-impedance outer loops and inner speed loops are the most popular. Reference [35] was presented a variable stiffness

The associate editor coordinating the review of this manuscript and approving it for publication was Min Wang.

control, suppressing the vibrations of a single-link robotic arm. An impedance-regulator control approach utilized a Markov chain to transit three modes [36], i.e., fixed, resistive, and passive. An H_∞ gain-scheduled controller was adopted to regulate the stiffness arbitrarily in some interval [37]. An acceleration-based controller solved the motion control problem of variable stiffness using two spring structures [38]. The optimal stiffness was predicted to be suitable for the peak power and energy requirements at different gaits [39]. An enhanced residual approach was used to estimate the external torques and widen the stiffness range [40]. Current SEA designs exhibit a common limitation in performance due to the spring stiffness.

Colgate applied passivity theory to study the stability of interaction [19], [41]. Reference [42] was presented a state-independent stability condition for varying stiffness and damping, which can be verified offline. Reference [43] used a tank-based approach to passive varying stiffness. The stiffness parameters of the above methods required both adjustment and interaction stability. The control methods mentioned above [23], [31]–[33], [36], [39], focus on constant-stiffness during a specific mode interaction. Furthermore, due to passivity restraints, the actual stiffness cannot exceed the physical stiffness. However, an impedance controller is proposed in this paper, in which the passive parameters and port stiffness can be relatively separated. The passive parameter should be recalculated via real-time stiffness to ensure interactive stability. Regulating the passive parameter is similar to the gain-scheduled method.

When processing the interaction with the SEA-driven robot, force, speed, and position are indicators of comfort and safety. Therefore, it is necessary to weigh these properties during the stiffness adjustment process. Stroke patients mainly perform muscular tension exercises in late rehabilitation. Rehabilitation robots are required to operate in different force application modes according to various muscle features, such as port impedance variations. Therefore, a design method must be developed to randomly adjust the port impedance and aid in muscle strength training. Thus, a hierarchical control scheme is adopted [44]. The upper layer is the stiffness predictive layer. The muscle stiffness during interactions is measured in real time, and a steady state optimization function is included. Then, output parameters are calculated by matching the muscle stiffness and port stiffness during interactions. The lower layer is the impedance control base layer, which has a cascade structure. The parameters of the controller are adjusted according to the output parameters in the upper layer for individualized strength training.

This paper proposes a novel control method for continuous stiffness adjustment in a one-DOF SEA-driven robot arm, and the main contributions are listed as follows. The stability and passivity criteria are derived from the impedance control law. The passivity still exists when the port stiffness is higher than the SEA physical spring. The predictive stiffness control method assesses the stiffness of human muscles in real-time and meets the constraint conditions associated with interaction stability, speed, and position. This method can be used to effectively adjust the port stiffness according to the muscle exercises. Both simulation and experimental results are presented to illustrate the performance of the proposed control method. The proposed stiffness adjustment algorithm can be used extensively in various SEA-driven robot systems, such as rehabilitation robots for human muscle exercise.

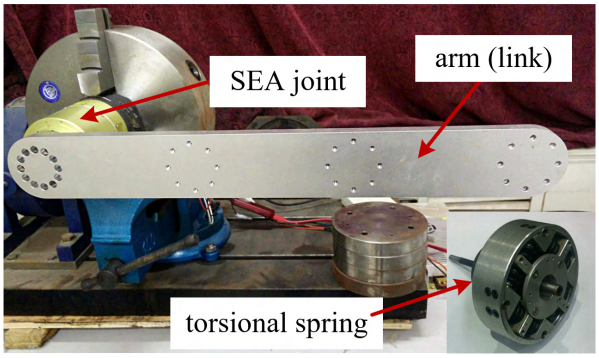

FIGURE 1. Robot arm driven by the SEA joint testing apparatus.

The rest of this paper is organized as follows. The SEA-driven robot arm model is presented in section II. The stiffness control method based on predictive control is discussed in section III. In section IV, the stability, passivity, port impedance and matching precision of the impedance controller are verified based on simulations. In section V, an experiment is conducted not only to examine the characteristics of port stiffness and the stiffness of human muscles but also to compare the port stiffness features during interactions with and without the predictive controller. Finally, the conclusions are given in section VI.

II. MODEL ANALYSIS

A. SEA-DRIVEN ROBOT ARM SETUP

An SEA joint with a spring structure typically adopts the series design method and fully considers coordination with the internal space size of the joint. In practical applications of rehabilitation robots, there are always mass connection components such as arms between the joint and the load or between the joints [45].

For the convenience of subsequent work, we designed an SEA-driven robot arm testing apparatus [46], [47], which is shown in Fig. 1. The elastic structure can be approximated as a torsional spring. According to the characteristics of the experimental platform and the expansion of the robotic arm (connections are generally used between the joints in the arm, which is similar to the linkage load of this model), we consider the SEA-driven robot arm model.

Robot models have nonlinearities and uncertainties. Discontinuous friction, which can be linearly parameterized, is compensated by an adaptive mechanism [24]. References [48] and [49] can overcome unknown time-delay functions and perturbed uncertainties. Reference [50] presents adaptive neural learning control for unknown robot dynamics

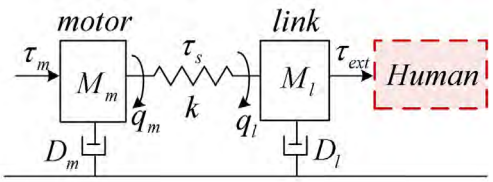

FIGURE 2. SEA-driven robot arm model.

under prescribed performance constraints. Reference [22] provides methods for estimating unknown parameters in the case of expansion to a multiple-DOF system. Reference [51] shows a linear analysis of the SEA model. To maintain the generality of the study, some design features, which vary from device to device, can be ignored without losing generality. In particular, the following assumptions [5], [9], [33] are summarized here as a reference:

1) Spring stiffness is considered to be linear since spring torque saturation is avoided during the experiment.
2) It is possible to develop a linear model by ignoring nonlinear friction and backlash.
3) Electric components can be ignored due to the high-frequency contributions.
4) Load inertia should be modeled since it affects the passive range for the interactive stability adjustment.
5) This paper discusses a one-DOF SEA-driven robot arm, which makes the dynamic parameters easy to ascertain.

B. MODEL OF THE SEA-DRIVEN ROBOT ARM

Fig. 2 shows the SEA-driven robot arm model. The dynamic model of the one-DOF SEA-driven arm can be expressed as:

$$\begin{cases} M_m\ddot{q}_m + D_m\dot{q}_m = \tau_m - \tau_s \\ M_l\ddot{q}_l + D_l\dot{q}_l = \tau_s + \tau_{ext} \\ \tau_s = k(q_m - q_l) \end{cases} \tag{1}$$

where the variables M_m and M_l are the motor and link inertia, respectively; k is the elastic spring stiffness; D_m and D_l are the motor and link friction coefficients, respectively; q_m is the motor position; q_l is the link (or joint) position; τ_m is the motor input force (or torque); τ_s is the spring force; and τ_{ext} is the external force.

The relationship between τ_m and τ_{ext} can be derived as follows:

$$\tau_m = -(1 + \frac{J_{motor}}{k})\tau_{ext} + (J_{motor} + J_{link})q_l + \frac{J_{motor}}{k}J_{link}q_l \tag{2}$$

where $J_{motor} = M_m s^2 + D_m s$ and $J_{link} = M_l s^2 + D_l s$.

The variable τ_m is composed of force-related terms, the motor-link kinetic energy and the energy related to elastic deformation.

We set $Z = \tau_{ext}/\dot{q}_l$, where Z is the port impedance. From (2), we can derive the following equation.

$$Z = \frac{J_{link}}{s} + \frac{1}{s[J_{motor}^{-1} + k^{-1}]} - \frac{k}{J_{motor} + k}\frac{\tau_m}{\dot{q}_l} \tag{3}$$

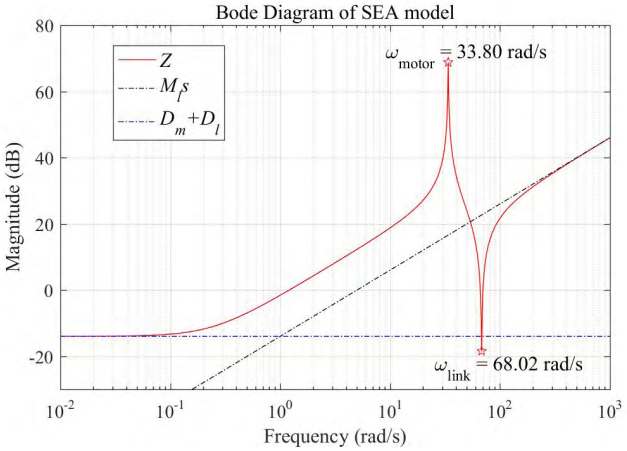

FIGURE 3. Uncontrolled SEA point impedance.

Setting $\tau_m = 0$, the response curve of port impedance without motor torque is drawn in Fig. 3, which clearly shows the motor resonance point $\omega_{motor} \approx (k/M_m)^{1/2}$ and the link resonance point $\omega_{link} \approx [k(M_m + M_l) / (M_m M_l)]^{1/2}$. The red solid line is uncontrolled $Z(s)$. The blue dotted line is the link inertia $D_m + D_l$, which is also the response of the port impedance at low frequencies. The black dotted line is the link inertia $M_l s$, which is also the response of the port impedance at high frequencies.

III. CONTROL STRUCUTRE

A novel variable-stiffness controller is illustrated in Fig. 4. Unlike traditional control methods, we add stiffness prediction in parallel based on the cascade control scheme to fit the muscle tension when performing rehabilitative training with robots. The input of the stiffness prediction is the spring force. Here, K_S is the desired stiffness, K_D is the desired damping, ε is the inner-loop gain, *kin p* is a proportionality parameter, *kin d* is a derivative parameter, and q_d is the desired position.

A. IMPEDANCE CONTROLLER

The impedance controller is governed by the following equation.

$$\tau_m = \varepsilon(k_p^{in} + k_d^{in}s)\,[(K_S + K_D s)(q_d - q_l) - \tau_s] + \tau_s \tag{4}$$

The closed-loop transfer function is as follows.

$$C_a(s) = \frac{q_l}{q_d} = k\frac{\varepsilon(k_p^{in} + k_d^{in}s)(K_S + K_D s)}{\sum_{i=0}^{4} n_i s^i} \tag{5}$$

in which

$$\begin{cases} n_0 = k\varepsilon K_S k_p^{in} \\ n_1 = k(\varepsilon D_l k_p^{in} + D_m + \varepsilon K_S k_d^{in} + \varepsilon K_D k_p^{in}) \\ n_2 = k\varepsilon M_l k_p^{in} + D_m D_l + k(M_m + \varepsilon k_d^{in} D_l + \varepsilon K_D k_d^{in}) \\ n_3 = M_l(D_m + k\varepsilon k_d^{in}) + D_l M_m \\ n_4 = M_l M_m \end{cases}$$

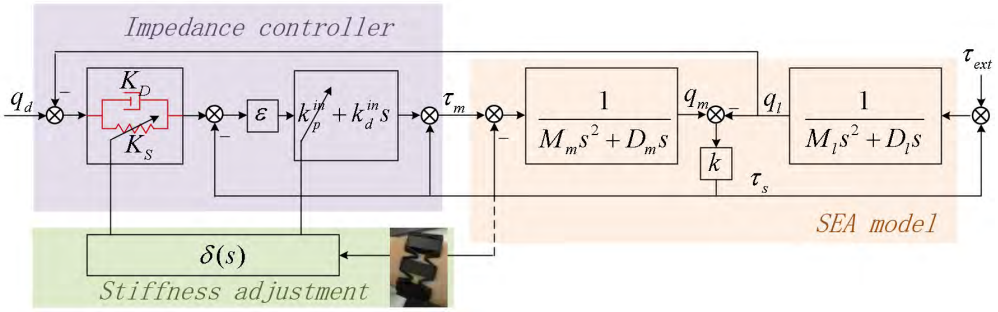

FIGURE 4. Variable-stiffness control structure.

The actual port impedance of the SEA is given by the following equation.

$$Z_a(s) = \frac{\tau_{ext}}{\dot{q}_l} = \frac{\sum_{i=0}^{4} n_i s^i}{M_m s^3 + (D_m + k\varepsilon k_d^{in}) s^2 + k\varepsilon k_p^{in} s} \tag{6}$$

The stability and passivity conditions of the impedance controller and the port stiffness formula are given below. These are the basic conditions for port prediction.

1) STABILITY

Characteristic (6) is the four-order equation. According to the Routh-Hurwitz criterion [52], the following conclusions can be obtained.

Theorem 1: System (6) is stable if the following inequalities hold: ($K_S > 0$, $K_D > 0$, $\varepsilon > 0$, $kin\ p > 0$,$kin\ d > 0$) and

$$n_3 n_2 - n_4 n_1 - n_3^2 n_0 n_1^{-1} > 0 \tag{7}$$

Corollary 1: There exists a value of $\varepsilon^* > 0$ such that system (5) is stable for all $\varepsilon \in [\varepsilon^*, \infty)$ when all controller parameters are positive. If D_m and D_l can be ignored, ε^* can be approximated as follows.

$$\varepsilon^* \approx \frac{M_m (K_S k_d^{in} + K_D k_p^{in})(K_S k_d^{in} + K_D k_p^{in} - k k_d^{in})}{k K_D k_d^{in} (M_l k_P^{in^2} + K_S k_d^{in^2} + K_D k_p^{in} k_d^{in})} \tag{8}$$

2) PASSIVITY

The passivity of the controlled robot is a sufficient and necessary condition that guarantees stable interactions with any passive environment [53].

Definition 1 [21]: A system defined by the linear 1-port impedance function $Z(s)$ is passive iff

1) $Z(s)$ has no poles in the right half-plane.

2) Any imaginary poles of $Z(s)$ are simple and have positive real residues.

3) $\mathrm{Re}\{Z(j\omega)\} \geq 0$.

Theorem 2: The actual port impedance $Z_a(s)$ is passive if the following conditions hold: ($K_S > 0$, $K_D > 0$, $\varepsilon > 0$, $kin\ p > 0$,$kin\ d > 0$) and

$$\mathrm{b} \geq 0 \text{ and } \mathrm{c} \geq 0, \text{ or } \mathrm{b} < 0 \text{ and } \mathrm{b}^2 - 4\mathrm{ac} \leq 0 \tag{9}$$

where

$$\begin{cases} a = D_l M_m^2 \\ b = D_m n_2 + k\varepsilon (k_d^{in} n_2 - k_p^{in} n_3) - M_m n_1 \\ c = k\varepsilon (k_p^{in} n_1 - k_d^{in} n_0) - D_m n_0 \end{cases}$$

Corollary 2: A value of $\varepsilon^{\#} > 0$ exists such that $Z_a(s)$ is positive for all $\varepsilon \in [\varepsilon^{\#}, \infty)$ when all controller parameters are positive. If D_m and D_l can be ignored, $\varepsilon^{\#}$ can be approximated as follow.

$$\varepsilon^{\#} \approx M_m \frac{K_S k_d^{in} - k k_d^{in} + K_D k_p^{in}}{k K_D k_d^{in^2}} \tag{10}$$

Based on a comparison of (8) and (10), we can obtain $\varepsilon^* < \varepsilon^{\#}$ by adjusting K_S and $\varepsilon > \varepsilon^{\#}$ for the impedance controller. These actions not only result in arbitrary values of port stiffness but also satisfy the interaction stability condition.

As ε grows, the port impedance performance is given as follows.

$$\tilde{Z}_a(s) \overset{\varepsilon \to \infty}{\approx} \frac{K_S}{s} + K_D + D_l + M_l s \tag{11}$$

B. STIFFNESS ADJUSTMENT

Section III.A deduces that K_S is the approximate value of the SEA port stiffness under the impedance controller, and the parameter ε guarantees the passivity. By adjusting these two parameters, the port stiffness of the SEA can be achieved and the interaction is stabilized. This section focuses on dynamically adjusting these two parameters to achieve the desired muscle exercise. Fig. 5 illustrates the process of stiffness adjustment. Here, K_{man} is the man muscle stiffness, and K_{port} is the desired port stiffness.

There are two points that must be set in advance: the desired port stiffness range and the stiffness optimization type. The desired range of port stiffness must be calibrated according to the stiffness of the experimenter's muscles. Obviously age and gender are the main factors affecting muscle stiffness.

Stiffness optimization is mainly based on the three muscle states of stroke patients [54], who have special muscle characteristics in different periods and requires the specific muscle exercises listed in Table 1 [55]–[59]. During the active

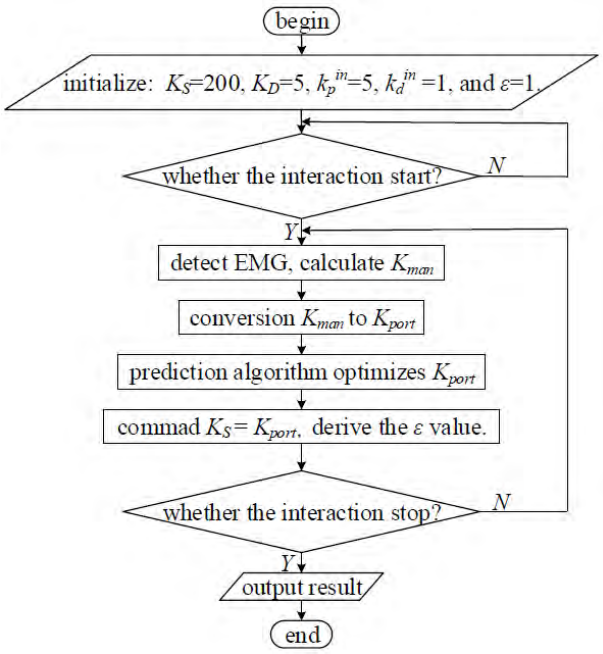

FIGURE 5. Stiffness adjustment.

TABLE 1. The muscle characteristics of the stroke.

Period	Ashworth	Need exercise
Soft	------	Fixed stiffness position training
Spasm	1+	Relaxation training
Active separation	1	Confrontation training

separation period, the muscle stiffness is proportional to the port stiffness; during the spasm period, the muscle stiffness is inversely proportional to the port stiffness; during the soft period, there is a force boundary point.

The following is an introduction to the algorithm in which the arm of a 25-year-old male requires muscle training during the active separation period.

1) PORT STIFFNESS RANGE ESTIMATION

First, the relationship between the applied force and the muscle stiffness must be calibrated to determine the range of port stiffness.

During rehabilitation training, the goal of muscle training is to exercise muscle tone to a healthy level. Thus, we need to know the tendon status of healthy people to develop a benchmark for muscle regulation. Section V.B shows a concrete example. The following equation is used for stiffness conversion:

$$K_{port} = \xi K_{man} \tag{12}$$

where ξ is the value set by the doctor according to the characteristics of the tendon. The doctor suggested that ξ could be set to 50 when the patient is in the first stage using the SEA-driven arm.

2) PREDICTION ADJUSTMENT

The purpose of stiffness prediction is to comprehensively consider the muscle stiffness, displacement and velocity error of training equipment within the specified range. The port stiffness is dynamically modified during training. Port stiffness delays during a sudden force increase or decrease are avoided.

The prediction process involves the real-time detection of port forces and muscle stiffness, the optimization of port stiffness, and the adjustment of the passivity margin. When muscle stiffness increases, port stiffness increases.

The impedance controller parameter K_S is automatically adjusted online by predictive estimations of the joint output response. The output value at the next time step $K_S(t+1)$ is predicted in the time domain based on the value of $K_S(t)$.

During the dynamic interaction process, the experimenter applied an external force on the SEA link, which would cause velocity and displacement at the link. If the stiffness of the port is different, the magnitude of the two quantities will be different. When the force application speed is high and the action time is short, detection via EMG alone is not perfect, perhaps because as the stiffness of the port increases, the muscles are already relaxed.

Therefore, the small delay in port stiffness adjustment can be avoided by adding the dynamic characteristic indicator equation of velocity and displacement, resulting in the following:

$$J = \min(q_l - \frac{\tau_s}{K_S(t+p-1|t)})^2 + \min(v_{ql} - v_{qld})^2 \tag{13}$$

where $K_S(t+p|\,t)$ represents the predicted value of K_S at time t at time step $t+p$, v_{ql} is the speed of the link and v_{qld} is the desired speed of the link. This paper takes the realistic value of p = 8 ms. The displacement offset is converted according to the real-time port impedance. Equation (13) is the deviation of velocity and displacement for minimizing the current port impedance.

This value can be quickly superimposed on the port stiffness when velocity and position offsets suddenly occur at the SEA device. The predicted modification is as follows.

$$K_S(t+p|t) = \sum_{i=1}^{p} J + K_S^{ref}(t+p|t) \tag{14}$$

where K_S^{ref} is K_{port}, which is calculated in the previous section.

During the actual rehabilitation training process, we must consider the amplitude constraint:

$$\begin{cases} \tau_{s.\min} \le \tau_s \le \tau_{s.\max} \\ K_S(t) \in \pm 20\% \xi \delta(\tau_s) \\ \varepsilon = trunc(\varepsilon^{\#} + 1) \end{cases} \tag{15}$$

where trunc(x) is the rounding function and ε ensures the passivity of the SEA system. $\delta(\tau_s)$ is variable for different populations. Section V.B provides a concrete example of the

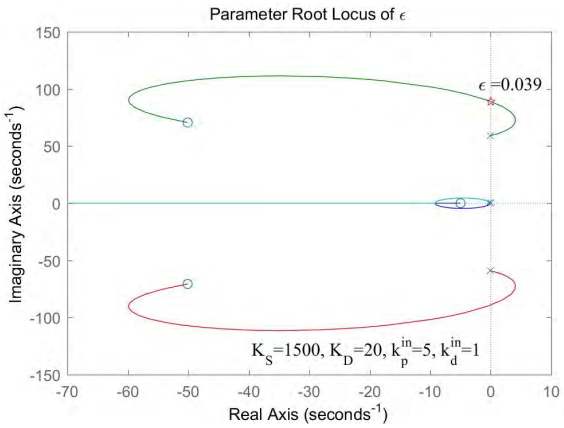

FIGURE 6. Parameter root locus of ε.

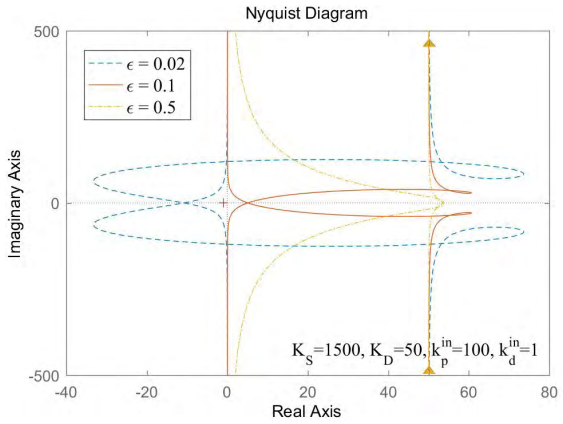

FIGURE 7. Nyquist diagram of Z_a (s).

$\delta(x)$ function. This paper applies the following values based on functionality: $\tau_{s.min} = 0$, and $\tau_{s.max} = 30$.

When the predicted value exceeds the reference input, the amount of control should be reduced to decrease the stiffness of the output. Conversely, if the predicted value is less than the parameter input, the amount of control should be increased. In stiffness prediction controller design, an electromyographic (EMG) sensor first performs muscle state detection and approximates the stiffness port range. When the robotic arm drives the human body during rehabilitation training, the predicted stiffness parameters K_S and ε will be adjusted according to the force applied by the human body to improve the rehabilitation effect.

IV. SIMULATION

A. STABILITY AND PASSIVITY

Fig. 6 presents the ε parameter root locus. Other parameters of the controller are listed in Fig. 6 as well. The approximate value of ε^* is 0.039. The data demonstrate that stability can be guaranteed as long as $\varepsilon \geq 0.039$.

Fig. 7 summarizes the Nyquist diagram of the actual port impedance $Z_a(s)$ for different ε values. The approximate value of $\varepsilon^{\#}$ is 0.100. The data demonstrate that the passivity conditions are guaranteed if $\varepsilon \geq 0.100$.

B. IMPEDANCE APPROXIMATION

1) COST VALUE

A cost function measuring the difference between $Z_a(s)$ and $Z_d(s)$ over various frequencies ω_1 to ω_2 is defined in (16). A log-log scale can effectively illustrate the magnitude range of values from low to high frequencies.

$$Cost = \int_{\omega_1}^{\omega_2} \log \frac{|Z_d(j\omega)|}{|Z_a(j\omega)|} d\omega \tag{16}$$

A grid of ε and K_S is uniformly drawn with 10^4 nodes in [1,1000] × [1,1000]. The target impedance is set as $Z_d(s) = K_S/'s + 50$. The frequencies are tested from 10^{-2} rad/s to 10^3 rad/s. The cost is proportional to a discrete approximation of the shaded area in Fig. 8, which illustrates the cost variations

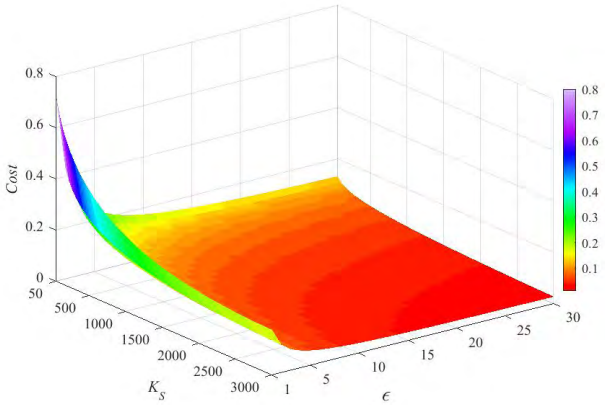

FIGURE 8. Distribution of cost variation with respect to ε and α.

TABLE 2. Comparison of four impedance methods.

Number	Control law	Port stiffness
①	$\tau_m = (P_1 + D_1 s)(q_d - q_m)$	$K_1 = \frac{kP_1}{k + P_1}$
②	$\tau_m = (P_2 + D_2 s)(q_d - q_l)$	$K_2 = P_2$
③	$\begin{cases} v_{qm} = (P_4 + \frac{I_2}{s})[P_3(q_d - q_E) - \tau_s] \\ \tau_m = (P_3 + \frac{I_1}{s})(v_{qm} - s q_m) \end{cases}$	$K_3 = P_3$
④	$\begin{cases} v_\tau = (K_S + K_D s)(q_d - q_l) \\ \tau_m = \varepsilon(k_p^{in} + k_d^{in} s)(v_\tau - \tau_s) + \tau_s \end{cases}$	$K_4 = K_S$

with respect to ε and K_S, assuming that the SEA system is stable and passive.

2) LOWER STIFFNESS

To illustrate the port stiffness characteristics of this impedance controller, Table 2 provides three common position controllers.

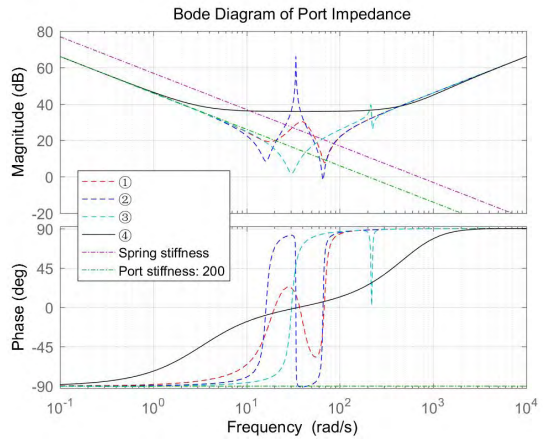

FIGURE 9. Comparison of the four methods.

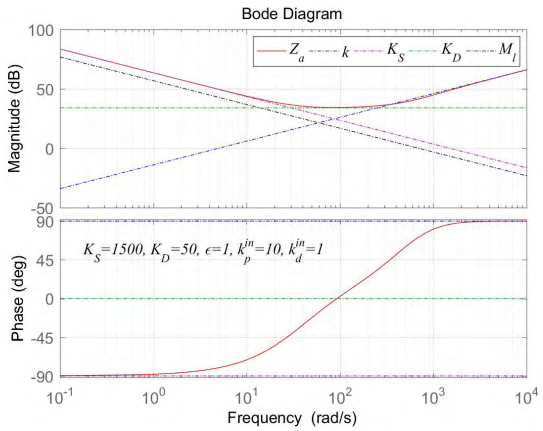

FIGURE 10. Bode diagram of Z_a (s).

To derive the port stiffness, q_d is set to 0, where P_i ($i = 1,\ldots,4$), D_1, D_2, I_1, and I_2 are the parameters of the former three controllers. The impedance controller in this article employs method ŕ. Method ň of the motor position feedback determines that its port stiffness value must be less than the physical spring stiffness value. Methods and ő imply that the SEA can display a lower stiffness than the physical spring stiffness if passivity is desired [5].

Fig. 9 shows the port impedance frequency response when the desired port stiffness value is 200. The pink dotted line refers to the physical spring stiffness of the SEA. All four methods mentioned above can achieve the desired stiffness under low frequency while also satisfying passivity. However, the former three methods occur the resonance in the middle frequency. Method ŕ does not display any resonance problems.

3) HIGHER STIFFNESS

Fig. 10 shows the frequency response curve of the SEA actual port impedance $Z_a(j\omega)$ (the controller parameters are marked in the figure). The design stiffness value is 1500 Nm/rad as shown by the black dotted line. Z_a(red solid line) approaches

TABLE 3. SEA parameter values.

Parameter	Value	Units
M_m	0.61	kg·m^2
M_l	0.20	kg·m^2
k	696.90	Nm/rad
D_m	0.15	Nm·s/rad
D_l	0.05	Nm·s/rad

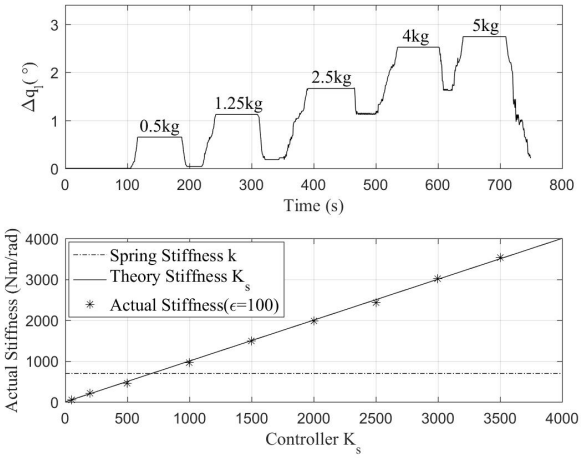

FIGURE 11. Stiffness characteristics.

the stiffnessK_S (pink dot line) at low frequencies, the damping K_D (green dot link) at intermediate frequencies, and the inertia M_l (blue dot link) at high frequencies. The system is passive because the phase range is $\pm 90°$.

It can be observed from Fig. 10 that when the port stiffness is greater than the physical spring stiffness, the system is still passive, and the impedance control method suppresses the resonance problem of the model itself.

V. EXPERIMENTS

As shown in Fig. 1, a testing apparatus featuring a flat arm (link) and an SEA joint is constructed. The parameter values associated with the rotary SEA prototype are provided in Table 3.

A. STIFFNESS CHARACTERISTICS OF THE IMPENDENCE CONTROLLER

The unloaded arm moves horizontally, and the weight disks are loaded in sequence. The virtual stiffness is calculated as follows: $k_s' = \Delta G/\Delta q_l$, where ΔG is the loading gravity torque and Δq_l is the resulting deflection. Fig. 11 depicts the link position fluctuations at $K_S = 500$ as the disks are loaded in sequence. The least squares method is used to calculate the stiffness K_S of the system port. When $\varepsilon = 100$, the actual stiffness value is approximately the same as the controller parameter K_S.

B. EMG SIGNAL

Fig. 12 illustrates a calibration process of force and EMG signals. During the experimental procedure, the average value

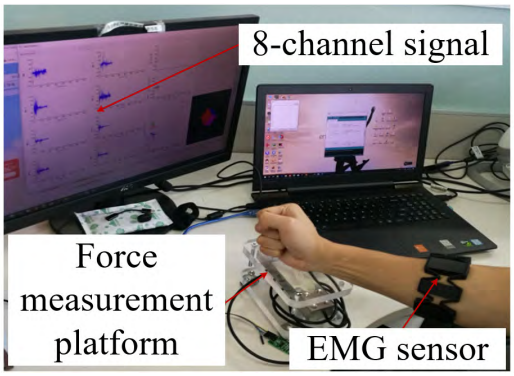

FIGURE 12. EMG signal calibration.

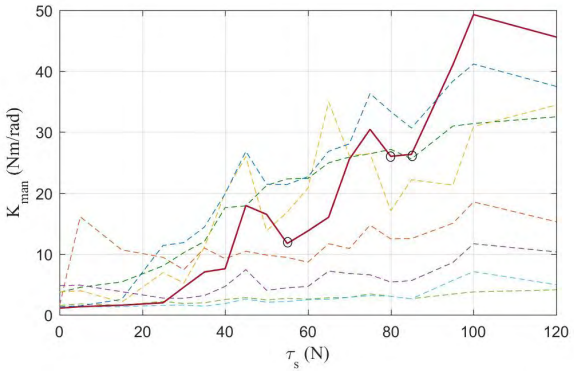

FIGURE 13. Muscle characteristics.

of the 8-channel signal data represents the muscle stiffness of the human body.

Fig. 13 shows the relationships between τ_s and K_{man}, as measured by an electromyographic (EMG) sensor. The line in the figure is the 8-channel signal acquisition. The pit-points marked with ''o'' on the curve denote muscle fatigue during exercise, which can be clearly seen in the demonstrated curve.

The port stiffness benchmark function (the black dotted line in Fig. 14 is the mean of the data in Fig. 14) is as follows:

$$\delta(x) = 41.5\sin(0.14x - 0.55) + 105\sin(0.207x + 1.915) + 75\sin(0.2254x + 4.85) + 1.32\sin(0.82x - 0.62) \quad (17)$$

Equation (17) is an example of this article. From (12) and (17), the relationship between the applied force and the port stiffness in Fig. 14 can be obtained, and ± 20% of the curve is selected as the desired port stiffness range.

During the experiment, when the expected value of the port stiffness falls within the dotted curve in Fig. 14, if it is less than this range, then it will increase; if it is greater than this range, then it will decrease. This range is the basis for ensuring effective and safe muscle training.

C. INTERACTIVE EXPERIMENT

SEA single-joint robots have their own applications, such as a simple variable stiffness rehabilitation rotary handle [32], [60]. During the experiment, the multi-joint robot arm cannot avoid the singular configuration and multi-joint

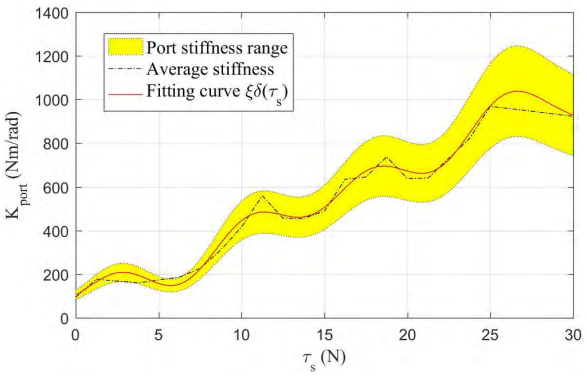

FIGURE 14. Port stiffness range.

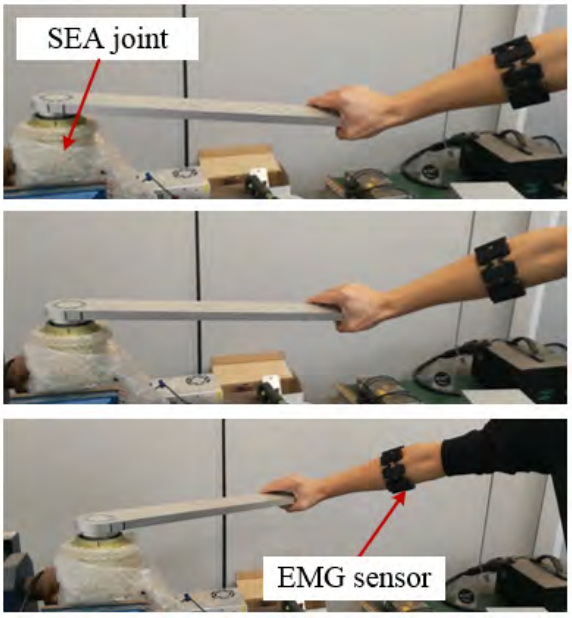

FIGURE 15. Motion process.

coupling, thus, the single joint is easier to use to verify the correctness of the algorithm.

According to the characteristics of muscle tension during the rehabilitation process, the port stiffness is adjusted by applying different forces. During muscle training, the volunteer used varied force to push and pull the platform arm in the experiment ($q_d = 0°$), as shown in Fig. 15.

Figs. 16 and 17 show the relationships among τ_s, q_l, v_{ql} and K_S during the motion experiment. Over time, τ_s increases, as does the arm muscle stiffness strength. The red dashed line shows the impedance controller without stiffness adjustment. The black solid line is the port stiffness value adjusted in real time based on the stiffness prediction. The blue dot-dashed line (no stiffness prediction) is the port stiffness value without stiffness prediction. As the external force increases, the positional deviation in q_l gradually increases. Due to the constant stiffness, if the port stiffness is small, then the force is easily increased. At this time, the experimenter did not feel muscle fatigue.

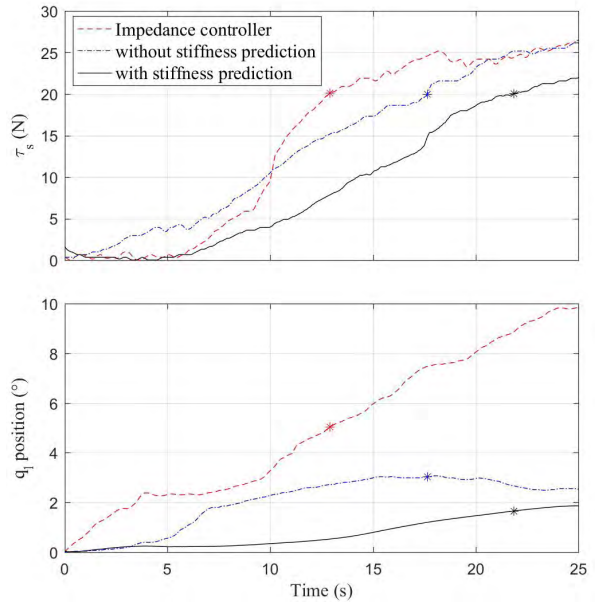

FIGURE 16. Motion comparison.

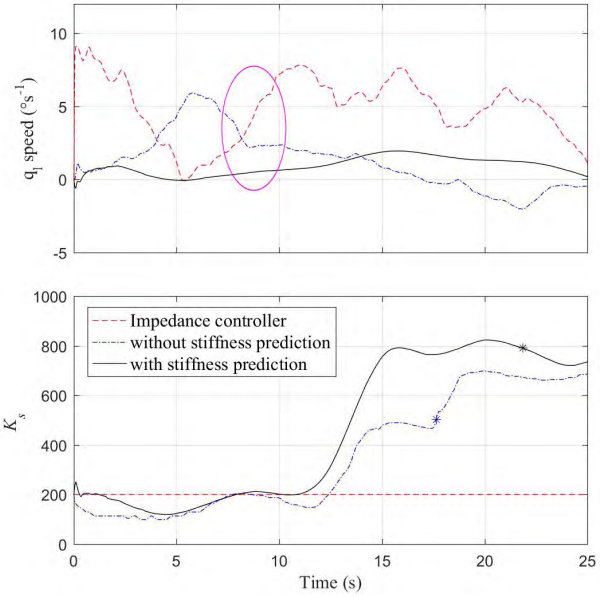

FIGURE 17. Stiffness comparison.

For example, assuming a fixed value of the external force of 20 N, the q_l position of 5° (when the port stiffness is 200) is required when there is no stiffness adjustment. The displacement is reduced to 3° without stiffness prediction (the port stiffness is changed to 503). In contrary, the displacement is reduced to only 1.6° with the stiffness prediction (the port stiffness is changed to 790).

Fig. 17 shows the different stiffness K_S values associated with the motion in Fig. 15. The addition of predictive control can effectively avoid delays and ensure a stable output port stiffness. Considering that the stiffness prediction increased from 12-15 s, the q_l speed is gentle. The other two methods vary greatly in speed. The speed variation is in the range from 0-9°/s with only impedance control. The speed variation is in the range from 0-6°/s without stiffness prediction. The speed variation is in the range from 0-2°/s with stiffness prediction.

Under the condition of stiffness prediction, and for the same force, the displacement was small, and the port stiffness increased. We can estimate the stiffness required for the interactive port by calculating the stiffness of the human body in real time. Because real-time motion speed and port stiffness tracking are considered, the volunteer does not have to rapidly increase the applied force.

The larger the force applied by the volunteer, the larger the port stiffness, and the muscles can be efficiently trained. This change in port stiffness makes it easy for the volunteer to exercise their muscles.

In our experiment, when the candidate has relatively high muscle tension, the port stiffness can be adjusted to increase the stiffness value K_S. Thus, according to the stiffness prediction, the muscles are comfortable during the process of upper limb rehabilitation.

VI. CONCLUSION

A parallel variable-stiffness control method is designed for upper limb rehabilitation training. The control method consists of two parts: the application of a series impedance controller to meet port stiffness and interaction stability requirements and stiffness prediction to forecast muscle tension at the contact moment and adjust the stiffness in real time. The cascade impedance controller can establish the stiffness of any port with passivity. Thus, the real-time stiffness adjustments satisfy the interactive stability requirements during the interaction process. In addition, stiffness prediction is added in parallel with the control scheme. According to the stiffness prediction, the relationship between muscle stiffness and external forces is given.

In this study, an SEA joint test platform is built to test the variable-stiffness adjustment process for the rehabilitation of an upper limb with the muscle training. In the experiment, taking the rehabilitation period as an example, the stiffness prediction achieves the same muscle tension with an increased force, and the proposed method performs better than the constant stiffness control approach. The experimental results indicate that the new algorithm is effective for variable-stiffness control based on the muscle tension of a patient. The method is expected to be applied to different muscles affected by stokes to self-adjust the stiffness.

When the stiffness prediction is adjusted, the male arm is taken as an example for illustration. However, this method is adaptable to groups of different genders and ages, as EMG signals are real-time signals and ξ can be modified during muscle training. Additionally, the experimental process is the same. It is undeniable that, if the state of muscles is strictly classified and the range of muscle stiffness is refined, then this method will be effective for muscle exercise. Obviously, this application is not the focus of this article. Our next step should extend the algorithm to the multi-joint SEA robot system.

REFERENCES

[1] G. A. Pratt and M. M. Williamson, "Series elastic actuators," in *Proc. IEEE/RSJ Int. Conf. Intell. Robots Syst.*, Pittsburgh, PA, USA, Aug. 1995, pp. 399–406.

[2] M. Wang, L. Sun, W. Yin, S. Dong, and J.-T. Liu, "Series elastic actuator torque control approach for interaction application," *Acta Autom. Sinica*, vol. 43, no. 8, pp. 1319–1328, 2017.

[3] S. Wolf *et al.*, "Variable stiffness actuators: Review on design and components," *IEEE/ASME Trans. Mechatronics*, vol. 21, no. 5, pp. 2418–2430, Oct. 2016.

[4] M. H. Tan and S. Wang, "Research progress on robotics," *Acta Automatica Sinica*, vol. 39, no. 7, pp. 963–972, Jul. 2013.

[5] H. Vallery, J. Veneman, E. V. Asseldonk, R. Ekkelenkamp, M. Buss, and H. V. D. Kooij, "Compliant actuation of rehabilitation robots," *IEEE Robot. Autom. Mag.*, vol. 15, no. 3, pp. 60–69, Sep. 2008.

[6] Z. Ju, C. Yang, and H. Ma, "Kinematics modeling and experimental verification of baxter robot," in *Proc. 33rd Chin. Control Conf.*, Nanjing, China, Jul. 2014, pp. 8518–8523.

[7] J. F. Veneman, R. Ekkelenkamp, R. Kruidhof, F. C. T. Van Der Helm, and F. C. T. Van Der Helm, "A series elastic- and Bowden-cable-based actuation system for use as torque actuator in exoskeleton-type robots," *Int. J. Robot. Res.*, vol. 25, no. 3, pp. 261–281, Mar. 2006.

[8] H. Yu, S. Huang, G. Chen, Y. Pan, and Z. Guo, "Human–robot interaction control of rehabilitation robots with series elastic actuators," *IEEE Trans. Robot.*, vol. 31, no. 5, pp. 1089–1100, Oct. 2015.

[9] F. Petit, A. Dietrich, and A. Albu-Schäffer, "Generalizing torque control concepts: Using well-established torque control methods on variable stiffness robots," *IEEE Robot. Autom. Mag.*, vol. 22, pp. 37–51, Dec. 2015.

[10] R. Ham, T. G. Sugar, B. Vanderborght, K. W. Hollander, and D. Lefeber, "Compliant actuator designs," *IEEE Robot. Autom. Mag.*, vol. 16, no. 3, pp. 81–94, Sep. 2009.

[11] N. L. Tagliamonte, F. Sergi, D. Accotom, G. Carpino, and E. Guglielmelli, "Double actuation architectures for rendering variable impedance in compliant robots: A review," *Mechatronics*, vol. 22, no. 8, pp. 1187–1203, Dec. 2012.

[12] L. C. Visser, S. Stramigioli, and A. Bicchi, "Embodying desired behavior in variable stiffness actuators," *IFAC Proc. Volumes*, vol. 44, no. 1, pp. 9733–9738, Jan. 2011.

[13] F. Petit, A. Daasch, and A. Albu-Schäffer, "Backstepping control of variable stiffness robots," *IEEE Trans. Control Syst. Technol.*, vol. 23, no. 6, pp. 2195–2202, Nov. 2015.

[14] D. Braun, M. Howard, and S. Vijayakumar, "Optimal variable stiffness control: Formulation and application to explosive movement tasks," *Auto. Robots*, vol. 33, no. 3, pp. 237–253, 2012.

[15] A. Zhakatayev, M. Rubagotti, and H. A. Varol, "Time-optimal control of variable-stiffness-actuated systems," *IEEE/ASME Trans. Mechatronics*, vol. 22, no. 3, pp. 1247–1258, Jun. 2017.

[16] B. Vanderborght *et al.*, "Variable impedance actuators: A review," *Robot. Auto. Syst.*, vol. 61, no. 12, pp. 1601–1614, 2013.

[17] J. W. Hurst, J. E. Chestnutt, and A. A. Rizzi, "The actuator with mechanically adjustable series compliance," *IEEE Trans. Robot.*, vol. 26, no. 4, pp. 597–606, Aug. 2010.

[18] N. Hogan, "Impedance control: An approach to manipulation: Part III—Applications," *J. Dynamic Syst. Meas. Control*, vol. 107, no. 1, pp. 17–24, Mar. 1985.

[19] J. E. Colgate and N. Hogan, "Robust control of dynamically interacting systems," *Int. J. Control*, vol. 48, no. 1, pp. 65–88, Jul. 1988.

[20] S. P. Buerger and N. Hogan, "Complementary stability and loop shaping for improved human–robot interaction," *IEEE Trans. Robot.*, vol. 23, no. 2, pp. 232–244, Apr. 2007.

[21] N. Hogan and S. P. Buerger, *Robotics and Automation Handbook*, vol. 19. Boca Raton, FL, USA: CRC Press, 2005, pp. 1–24.

[22] X. Li, Y. Pan, G. Chen, and H. Yu, "Adaptive human–robot interaction control for robots driven by series elastic actuators," *IEEE Trans. Robot.*, vol. 33, no. 1, pp. 169–182, Feb. 2017.

[23] C. Liu, C. C. Cheah, and J. J. E. Slotine, "Adaptive task-space regulation of rigid-link flexible-joint robots with uncertain kinematics," *Automatica*, vol. 44, no. 7, pp. 1806–1814, 2008.

[24] Y. Pan, H. Wang, X. Li, and H. Yu, "Adaptive command-filtered backstepping control of robot arms with compliant actuators," *IEEE Trans. Control Syst. Technol.*, vol. 26, no. 3, pp. 1149–1156, Mar. 2018.

[25] S. Nicosia and P. Tomei, "A method to design adaptive controllers for flexible joint robots," in *Proc. IEEE Int. Conf. Robot. Autom.*, Nice, France, May 1992, pp. 701–706.

[26] H. Yu, S. Huang, G. Chen, and N. Thakor, "Control design of a novel compliant actuator for rehabilitation robots," *Mechatronics*, vol. 23, no. 8, pp. 1072–1083, Dec. 2013.

[27] X. Li, Y. Pan, G. Chen, and H. Yu, "Multi-modal control scheme for rehabilitation robotic exoskeletons," *Int. J. Robot. Res.*, vol. 36, no. 5–7, pp. 759–777, Jun. 2017.

[28] A. Zhakatayev, M. Rubagotti, and H. A. Varol, "Closed-loop control of variable stiffness actuated robots via nonlinear model predictive control," *IEEE Access*, vol. 3, pp. 235–248, 2015.

[29] Y. Yan, C. Zhang, A. Narayan, J. Yang, S. Li, and H. Yu, "Generalized dynamic predictive control for nonparametric uncertain systems with application to series elastic actuators," *IEEE Trans Ind. Informat.*, vol. 14, no. 11, pp. 4829–4840, Nov. 2018.

[30] Y.-G. Xi, D.-W. Li, and S. Lin, "Model predictive control—Status and challenges," *Acta Automatica Sinica*, vol. 39, no. 3, pp. 222–236, Mar. 2013.

[31] G. A. Pratt, P. Willisson, C. Bolton, and A. Hofman, "Late motor processing in low-impedance robots: Impedance control of series-elastic actuators," in *Proc. Amer. Control Conf.*, Boston, MA, USA, Jun./Jul. 2004, pp. 3245–3251.

[32] A. Calanca and P. Fiorini, "A rationale for acceleration feedback in force control of series elastic actuators," *IEEE Trans. Robot.*, vol. 34, no. 1, pp. 48–61, Feb. 2018.

[33] N. L. Tagliamonte and D. Accoto, "Passivity constraints for the impedance control of series elastic actuators," *Proc. Inst. Mech. Eng., I, J. Syst. Control Eng.*, vol. 228, no. 3, pp. 138–153, Mar. 2014.

[34] G. Lin, X. Zhao, and J. Han, "A novel stiffness control method for series elastic actuator," in *Proc. 7th Int. Conf. Electron. Inf. Eng.*, Nanjing, China, Jan. 2017, pp. 1–8.

[35] A. Warkentin and S. E. Semercigil, "Variable stiffness control of a single-link flexible robotic arm," *J. Sound Vib.*, vol. 187, no. 1, pp. 1–21, Oct. 1995.

[36] A. L. Jutinico, J. C. Jaimes, F. M. Escalante, J. C. Perez-Ibarra, M. H. Terra, and A. A. G. Siqueira, "Impedance control for robotic rehabilitation: A robust markovian approach," *Frontiers Neurorobot.*, vol. 11, p. 43, Aug. 2017.

[37] N. Abroug and E. Laroche, "Transforming series elastic actuators into variable stiffness actuators thanks to structured H-infinity control," in *Proc. Eur. Control Conf.*, Linz, Austria, Jul. 2015, pp. 734–740.

[38] E. Sariyildiz, G. Chen, and H. Yu, "An acceleration-based robust motion controller design for a novel series elastic actuator," *IEEE Trans. Ind. Electron.*, vol. 63, no. 3, pp. 1900–1910, Mar. 2016.

[39] M. Grimmer and A. Seyfarth, "Stiffness adjustment of a series elastic actuator in an ankle-foot prosthesis for walking and running: The trade-off between energy and peak power optimization," in *Proc. IEEE Int. Conf. Robot. Autom.*, Shanghai, China, May 2011, pp. 1439–1444.

[40] J. Lee, C. Lee, N. Tsagarakis, and S. Oh, "Residual-based external torque estimation in series elastic actuators over a wide stiffness range: Frequency domain approach," *IEEE Robot. Autom. Lett.*, vol. 3, no. 3, pp. 1442–1449, Jul. 2018.

[41] H. Vallery, R. Ekkelenkamp, H. van der Kooij, and M. Buss, "Passive and accurate torque control of series elastic actuators," in *Proc. IEEE/RSJ Int. Conf. Intell. Robots Syst.*, San Diego, CA, USA, Oct./Nov. 2007, pp. 3534–3538.

[42] K. Kronander and A. Billard, "Stability considerations for variable impedance control," *IEEE Trans. Robot.*, vol. 32, no. 5, pp. 1298–1305, Oct. 2017.

[43] F. Ferraguti, C. Secchi, and C. Fantuzzi, "A tank-based approach to impedance control with variable stiffness," in *Proc. IEEE Int. Conf. Robot. Autom.*, Karlsruhe, Germany, May 2013, pp. 4948–4953.

[44] T. Zou, H. Pan, B.-C. Ding, and H.-B. Yu, "Research development of two-layered predictive control," *Control Theory Appl.*, vol. 31, no. 10, pp. 1327–1337, Oct. 2014.

[45] S. Moberg, J. Öhr, and S. Gunnarsson, "A benchmark problem for robust feedback control of a flexible manipulator," *IEEE Trans. Control Syst. Technol.*, vol. 17, no. 6, pp. 1398–1405, Nov. 2009.

[46] S. Li, J. Li, S-Q. Li, and Z.-L. Huang, "Design and implementation of robot serial integrated rotary joint with safety compliance," *J. Central South Univ.*, vol. 24, no. 6, pp. 1307–1321, Jun. 2017.

[47] G. Li *et al.*, "An innovative robotic training system imitating the cervical spine behaviors during rotation–traction manipulation," *Robot. Auton. Syst.*, vol. 107, pp. 116–128, Sep. 2018.

[48] M. Wang, X. Liu, and P. Shi, "Adaptive neural control of pure-feedback nonlinear time-delay systems via dynamic surface technique," *IEEE Trans. Syst., Man, Cybern. B, Cybern.*, vol. 41, no. 6, pp. 1681–1692, Dec. 2011.
[49] M. Wang, S. S. Ge, and K.-S. Hong, "Approximation-based adaptive tracking control of pure-feedback nonlinear systems with multiple unknown time-varying delays," *IEEE Trans. Neural Netw.*, vol. 21, no. 11, pp. 1804–1816, Nov. 2010.
[50] M. Wang and A. Yang, "Dynamic learning from adaptive neural control of robot manipulators with prescribed performance," *IEEE Trans. Syst., Man, Cybern., Syst.*, vol. 47, no. 8, pp. 2244–2255, Aug. 2017.
[51] W. Roozing, J. Malzahn, N. Kashiri, D. G. Caldwell, and N. G. Tsagarakis, "on the stiffness selection for torque-controlled series-elastic actuators," *IEEE Robot. Autom. Lett.*, vol. 2, no. 4, pp. 2255–2262, Oct. 2017.
[52] G. F. Franklin, J. D. Powell, and A. E.-Naeini, *Feedback Control of Dynamic Systems*, 7th ed. London, U.K.: Pearson, 2014, pp. 149–156.
[53] A. Van Der Schaft, "*L_2-Gain and Passivity Techniques in Nonlinear Control*, 3rd ed. Berlin, Germany: Springer, 2017, pp. 123–136.
[54] R. Colombo *et al.*, "Robotic techniques for upper limb evaluation and rehabilitation of stroke patients," *IEEE Trans. Neural Syst. Rehabil. Eng.*, vol. 13, no. 3, pp. 311–324, Sep. 2005.
[55] J. K. Ewoldt, E. C. Lazzaro, E. J. Roth, and N. L. Suresh, "Quantification of a single score (1+) in the modified Ashworth scale (MAS), a clinical assessment of spasticity," in *Proc. 38th Annu. Int. Conf. IEEE Eng. Med. Biol. Soc. (EMBC)*, Orlando, FL, USA, Aug. 2016, pp. 1737–1740.
[56] K. Li, W. Su, and L. Chen, "Performance analysis of three-dimensional differential geometric guidance law against low-speed maneuvering targets," *Astrodynamics*, vol. 2, no. 3, pp. 233–247, Sep. 2018.
[57] T. Zhang, "Chinese stroke rehabilitation guide," *China J. Rehabil. Theory Pract.*, vol. 18, no. 4, pp. 301–318, 2012.
[58] E. D. Vlugt, J. H. de Groot, K. E. Schenkeveld, J. Arendzen, F. C. van Der Helm, and C. G. Meskers, "The relation between neuromechanical parameters and Ashworth score in stroke patients," *J. NeuroEng. Rehabil.*, vol. 7, no. 35, pp. 1–16, Dec. 2010.
[59] Y. Ren and J. Shan, "Calibration of atmospheric density model using two-line element data," *Astrodynamics*, vol. 2, no. 1, pp. 13–24, Mar. 2018.
[60] B. Siciliano and O. Khatib, *Springer Handbook of Robotics*. Berlin, Germany: Springer, 2008, pp. 1229–1231.

SIQI LI was born in Langfang, Heibei, China, in 1984. She received the B.E. degree in automation engineering from the Hebei University of Science and Technology, Shijiazhuang, Heibei, in 2007, and the master's degree in mechanical engineering from the Taiyuan University of Science and Technology, Taiyuan, Shanxi, China, in 2011. She is currently pursuing the Ph.D. degree with the Beijing Institute of Technology, Beijing, China.

Her research interests include the robust control and control for rehabilitation robots.

JIAN LI received the B.E. and master's degrees in mechanical engineering from Beijing Technology and Business University, Beijing, China, in 2006 and 2010, and the Ph.D. degree in mechanical engineering from the Beijing Institute of Technology, Beijing, China, in 2015. He has been an Engineer with the School of Automation, Beijing Institute of Technology, since 2015.

His research interests include modeling and design of robotics, high-precision servo systems, game theory control, and predictive control.

GUIHUA TIAN received the Ph.D. degree from the Beijing University of Chinese Medicine, Beijing, China, in 2012.

She was a Visiting Scholar with the University of Toronto, Canada. She is currently an Associate Chief Physician, Associate Researcher, and a Master Tutor with the Dongzhimen Hospital, Beijing University of Chinese Medicine. Her research interests include clinical evidence, evaluation method, and effect mechanism of combination of acupuncture and medication in the prevention and treatment of chronic pain.

Dr. Tian was a winner of the Beijing Nova Program of Science and Technology and the winner of the Talents of China Association of Traditional Chinese Medicine.

HONGCAI SHANG received the Ph.D. degree from the Tianjin University of Traditional Chinese Medicine, Tianjin, China, in 2005.

He was a Researcher and a Doctoral Supervisor. He was the Deputy Director of the Beijing University Cardiology Research Institute of Traditional Chinese Medicine. He is currently the Director of the Key Laboratory of Chinese Internal Medicine of Ministry of Education, and the first Associate Dean of the Dongzhimen Hospital, Beijing University of Chinese Medicine. His research interests include the evaluation of traditional Chinese medicine (TCM) clinical evidence, and the characteristics and mechanism of their taking effect.

Dr. Shang received the National Science Fund for Distinguished Young Scholars.